

Chemical Science

Accepted Manuscript

This article can be cited before page numbers have been issued, to do this please use: E. Cariati, E. Lucenti, A. Forni, A. Previtali, D. Marinotto, D. Malpicci, S. Righetto, C. Giannini, T. Virgili, P. Kabacinski, L. Ganzer, U. Giovannella and C. Botta, *Chem. Sci.*, 2020, DOI: 10.1039/D0SC02459G.



This is an Accepted Manuscript, which has been through the Royal Society of Chemistry peer review process and has been accepted for publication.

Accepted Manuscripts are published online shortly after acceptance, before technical editing, formatting and proof reading. Using this free service, authors can make their results available to the community, in citable form, before we publish the edited article. We will replace this Accepted Manuscript with the edited and formatted Advance Article as soon as it is available.

You can find more information about Accepted Manuscripts in the [Information for Authors](#).

Please note that technical editing may introduce minor changes to the text and/or graphics, which may alter content. The journal's standard [Terms & Conditions](#) and the [Ethical guidelines](#) still apply. In no event shall the Royal Society of Chemistry be held responsible for any errors or omissions in this Accepted Manuscript or any consequences arising from the use of any information it contains.

Unravelling the intricate photophysical behavior of 3-(pyridin-2-yl)triimidazotriazine AIE and RTP polymorphs

Received 00th January 20xx,
Accepted 00th January 20xx

DOI: 10.1039/x0xx00000x

Elena Lucenti,^a Alessandra Forni,^{*a} Andrea Previtali,^{‡ab} Daniele Marinotto,^{‡a} Daniele Malpicci,^b Stefania Righetto,^{‡b} Clelia Giannini,^b Tersilla Virgili,^c Piotr Kabacinski,^c Lucia Ganzer,^c Umberto Giovanella,^d Chiara Botta,^{*d} and Elena Cariati^{*ab}

The development of purely organic materials showing multicolor fluorescent and phosphorescent behaviour represents a formidable challenge in view of practical applications. Herein the rich photophysical behaviour of 3-(pyridin-2-yl)triimidazotriazine (**TT-Py**) organic molecule, comprising excitation-dependent fluorescence and phosphorescence under ambient conditions in both blended film and crystalline phase, is investigated by means of steady state, time resolved and ultrafast spectroscopies and interpreted on the basis of X-ray diffraction studies and DFT/TDDFT calculations. In particular, by proper excitation wavelength, dual fluorescence and dual phosphorescence of molecular origin can be observed together with low energy phosphorescences resulting from aggregate species. It is demonstrated that the multiple emission property is originated by the copresence, in the investigated system, of an extended polycyclic nitrogen-rich moiety (**TT**), strongly rigidified by π - π stacking interactions and short C-H...N hydrogen bonds, and a fragment (**Py**) featuring partial conformational freedom.

Introduction

Purely organic materials showing Room Temperature Phosphorescence (RTP) in air have attracted attention in the last decade owing to the benefits they offer, including biocompatibility and low cost, compared to the widespread used phosphorescent inorganic materials. Organic RTP applications in several fields such as bioimaging, [1] anti-counterfeiting [2], catalysis [3] and displays [4] are emerging. Several strategies have been developed to realize organic RTP materials spanning from molecular engineering [5-7] to proper supramolecular organization based for example on H-aggregation [8-10] host-guest systems [11], halogen bonding, [12,13] and doping in polymer matrix [14]. Following these methods, some materials with long lifetime and high quantum yield have been effectively prepared. However, most of them can emit, according to the Kasha's rule, only from the lowest triplet level, resulting in one color emission. Very interesting are RTP materials able to cover a wide range of emission colors by simply varying the excitation wavelength. This has been achieved very rarely, e.g. by manipulation of intermolecular interactions to generate multiple color-tunable RTP emitting centres in a single-component molecular crystal [15] or, very recently, amorphous polymeric films of polyphosphazene derivatives into poly(vinyl alcohol) [16]. However, excitation dependent emissive behaviour is a very tricky subject which needs to be treated very carefully since, often, artifacts are at the basis of multiple emission from a hypothetical single

chromophore (see for example [17], [18] and references therein).

We have previously reported on the intriguing photophysical behaviour of a very simple, small, nitrogen rich organic molecule, namely triimidazo[1,2-a:1',2'-c:1'',2''-e][1,3,5]triazine, **TT** [9], and its Br- and I-derivatives [10, 19, 20]. **TT** is characterized by Aggregation-Induced Emission behavior, displaying in particular ultralong phosphorescence (RTUP) (1 s) at ambient conditions associated with the presence of H-aggregates in the crystalline structure [8]. The presence of one or multiple heavy (Br and I) atoms on the **TT** scaffold greatly modifies both its molecular and solid state photophysical behavior resulting in a complex excitation dependent photoluminescence with emissions comprising dual fluorescence, molecular phosphorescence, supramolecular RTP and RTUP, covering a wide portion of the visible region [10, 19, 20]. We have then moved towards preparation of new **TT**-derivatives characterized by intense, low energy and long lasting RTP for biological applications such as lifetime imaging [21]. To this aim, we have introduced on the trimidazolic scaffold suitable chromophoric fragments to shift the emission towards the red while preserving the long lifetime of the triplet state. Encouraging results in this direction have just been obtained with **TT-4pyF**, 3-(2-fluoropyridin-4-yl)triimidazo[1,2-a:1',2'-c:1'',2''-e][1,3,5]triazine, obtained by inserting the 2-fluoropyridine moiety on **TT** [21]. This compound possesses molecular fluorescence and green phosphorescence together with aggregate RTUP at almost 600 nm. These multiple emissions are collectively activated in the solid compound with an overall quantum efficiency Φ of 25%, showing that the 2-fluoropyridine fragment provides increased molecular performances with respect to **TT** itself, comprising fluorescence and heavy atom free phosphorescence, but it preserves the solid state RTUP which is shifted to the red (by about 70 nm) with respect to the **TT** parent compound [21].

Here we report on the multifaceted emissive properties of 3-(pyridin-2-yl)triimidazotriazine (**TT-Py**), the pyridine derivative

^a Institute of Sciences and Chemical Technologies "Giulio Natta" (SCITEC) of CNR, via Golgi 19, 20133 Milano, Italy

^b Department of Chemistry, Università degli Studi di Milano and INSTM RU, via Golgi 19, 20133 Milano, Italy

^c IFN-CNR, Dipartimento di Fisica, Politecnico di Milano, Piazza Leonardo da Vinci 32, I-20133 Milano, Italy

^d Institute of Sciences and Chemical Technologies "Giulio Natta" (SCITEC) of CNR, via Corti 12, 20133 Milano, Italy

[†] Electronic Supplementary Information available: NMR and mass spectra, photophysical data and spectra, single crystal X-ray crystallographic data, theoretical details and CIF files. See DOI: 10.1039/x0xx00000x

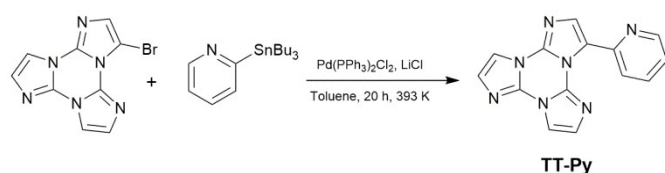
[‡] These authors contributed equally.



of **TT** where the nitrogen atom is located in ortho position with respect to **TT**. It will be demonstrated how this particular geometrical disposition is responsible for different metastable states which result, in the crystalline phase, in the formation of three polymorphs and in aggregated phase in a peculiar photophysical behaviour. In fact, excitation dependent emission is observed comprising dual fluorescence and multiple RTP even in blended films.

Results and discussion

TT-Py has been prepared by Stille coupling between 3-bromotriimidazo[1,2-*a*:1',2'-*c*:1'',2''-*e*][1,3,5]triazine and 2-(tributylstannyl)pyridine (Scheme 1) and characterized by NMR spectroscopy, mass spectrometry and X-ray analysis (see Supporting Information). The compound was recrystallized three times before photophysical characterization in order to avoid signals due to impurities.



Scheme 1 Synthesis of **TT-Py**

Diluted solutions of **TT-Py** (10^{-5} M) in acetonitrile (CH_3CN) and dichloromethane (CH_2Cl_2) in air at 298 K display absorption bands at about 235 and 290 nm and emission around 350 nm ($\Phi \cong 17\%$; Fig. 1). Surprisingly, lifetime measurements at 355 nm reveal both a short (ns) and a long (ms) lived character (see Table 1, Fig. S8-S9[†]). Moreover, while no other bands are visible in the PL (photoluminescence) spectrum, long lived components appear in both solvents when monitoring lifetimes at 400 and 500 nm ($\lambda_{\text{exc}} = 300$ nm, Fig. S10-S11[†]). To better understand this observation, we analyzed both steady state and time resolved spectra of deaerated solutions.

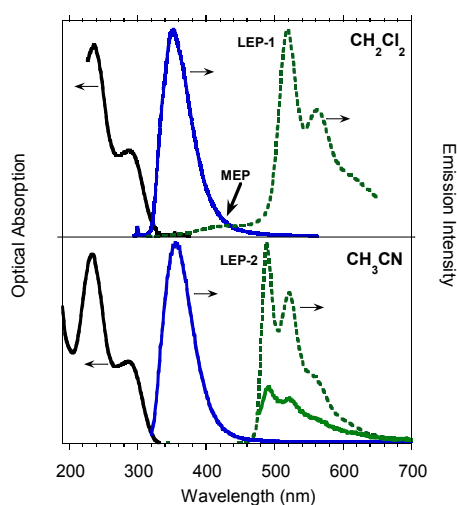


Fig. 1 Normalized optical absorption (black solid line) and PL spectra of 10^{-5} M deaerated solutions of **TT-Py** in CH_2Cl_2 (top) and CH_3CN (bottom) at 298 K. Top: blue solid line $\lambda_{\text{exc}} = 270$ nm; Bottom: blue solid line $\lambda_{\text{exc}} = 300$ nm; green solid line, $\lambda_{\text{exc}} = 390$ nm. Phosphorescence spectra of CH_2Cl_2 (top) (dotted green line, delay 50 μs , window 100 μs) and CH_3CN (bottom) (dotted green line, delay 200 μs , window 500 μs) $\lambda_{\text{exc}} = 300$ nm.

Time gated spectra of the CH_2Cl_2 solution show a broad band peaked at about 420 nm (medium energy phosphorescence, **MEP**, $\tau_{\text{av}} = 40$ μs) and a structured band at lower energy (low energy phosphorescence, **LEP-1**, $\tau = 441$ μs) with peaks at 520 and 562 nm (see Fig. 1 top and Fig. S12-S13[†]). Both phosphorescences are easily quenched through oxygen diffusion inside the cell (see Fig. S14[†]). A similar structured, but blue-shifted, **LEP** (**LEP-2**, peaks at 488, 521 and 560 nm) is observed in deaerated CH_3CN solutions (see Fig. 1 bottom) both in time gated spectra and in steady state measurements by selective excitation at 390 nm. The nature of the two **LEPs** has been investigated by forcing aggregation in CH_3CN through water addition. By exciting at 390 nm the nanoaggregated $\text{CH}_3\text{CN}/\text{H}_2\text{O}$ ($v/v = 50/50$) deaerated solution, the **LEP-2** spectral shape is recognized in the steady state spectrum (Fig. 2, Table 1). Accordingly, a 390 nm weak band appears in the excitation profile (PLE) of this emission (Fig. 2, green dotted line) while it is lacking in the absorption spectrum. Time gated spectra (Fig. 2 lower panel), however, display the same structured **LEP-1** observed in CH_2Cl_2 , together with an additional emission at about 345 nm (high energy phosphorescence, **HEP**) with lifetimes shorter than those of **MEP** centred at 380-420 nm. These results suggest that the two **LEPs** coexist in $\text{CH}_3\text{CN}/\text{H}_2\text{O}$ solutions and could be associated with the presence of different aggregated forms. To better summarize: the long lived emissions of the present system comprise two molecular components at high and medium energy (**HEP** and **MEP**) and a low energy one (**LEP**), associated to aggregated species. This latter can result in two slightly different emissions (**LEP-1** and **LEP-2**) depending on aggregation features.

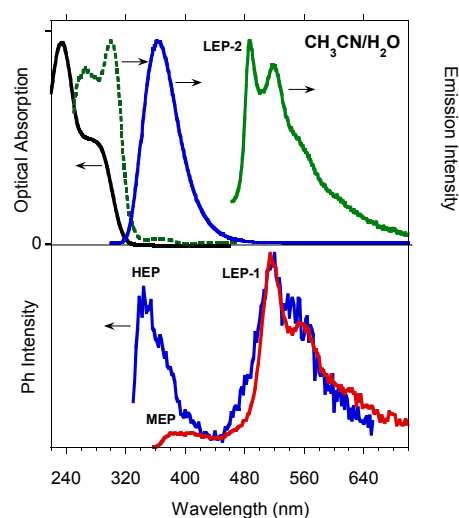


Fig. 2 Photophysical properties of deaerated solutions of **TT-Py** in 10^{-4} M $\text{CH}_3\text{CN}/\text{H}_2\text{O}$ ($v/v=50/50$) solution at 298 K. Top: Absorption (black solid line), PLE (green dashed line), emission (green solid line). Bottom: Absorption (black solid line), PLE (green dashed line), emission (red solid line).



line, $\lambda_{em}=488$ nm) and PL spectra (blue solid line, $\lambda_{exc}=270$ nm, green solid line, $\lambda_{exc}=390$ nm). Bottom: Phosphorescence spectra (blue line, delay 100 μ s, window 200 μ s; red line, delay 0.5 ms, window 1 ms, $\lambda_{exc}=300$ nm).

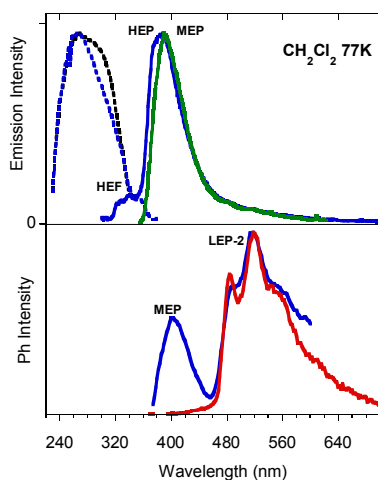


Fig. 3 Photophysical properties of 10^{-5} M CH_2Cl_2 solution of **TT-Py** at 77 K. Top: PL and PLE spectra ($\lambda_{em}=350$ nm, black dotted line; $\lambda_{em}=400$ nm, blue dotted line; $\lambda_{exc}=280$ nm, blue solid line, $\lambda_{exc}=350$ nm, green solid line). Bottom: Phosphorescence spectra, $\lambda_{exc}=350$ nm (delay 200 μ s, window 400 μ s, blue line; delay 10 ms, window 20 ms, red line).

Low temperature experiments have then been performed at 77 K. In CH_2Cl_2 an excitation dependent PL spectrum is observed (see Fig. 3 and Fig. S21[†]): a structured emission at about 340 nm (high energy fluorescence, **HEF**, $\tau_{av} = 2.32$ ns, Fig. S22[†]) together with the **HEP** component at about 375 nm are observed by exciting at 280 nm. At lower energy excitation (λ_{exc} 350 nm) the **MEP** emission appears at 393 nm (13.16 ms, Fig. S23[†]). Time gated emission measurements reveal a phosphorescence band peaked at 405 nm (**MEP**) associated to a shoulder in the excitation spectrum at about 350 nm. The longer lived (1.31 s, Fig. S24[†]) structured phosphorescence resembles the **LEP-2** spectral shape (485, 520, 555 nm). Broader spectra are observed by exciting at shorter wavelengths (300 and 325 nm, Fig. S25[†]). Similar results are observed by lowering the temperature in other solvents (CH_3CN and $\text{CH}_3\text{OH}/\text{CH}_3\text{CH}_2\text{OH}$ (v/v = 20/80), see Fig. S26-S30[†]).

In order to get deeper insight into the compound's photophysics and explore its applicative potential in the field of organic light emitting diodes (OLED, S31[†]), we prepared and characterized blended thin films of **TT-Py** in PMMA (w/w **TT-Py**/PMMA 10% and 5%). The already rich photoluminescence of the compound becomes even more complicated, displaying four different emissions which cover a large area of the PL spectrum (from 350 to 500 nm, Fig. 4, Table 2), regardless the film concentration. These emissions can be selectively activated by proper choice of the excitation wavelength. In particular, by exciting at high energy (below 300 nm) an intense fluorescent emission (**HEF**, $\tau = 1.18$ ns) at 350 nm dominates the spectrum. At 350 nm excitation, the **MEP** phosphorescence (13.73 ms) at 394 nm is observed. Surprisingly, an additional prompt emission band at 440 nm

(3.47 ns, low energy fluorescence, **LEF**) appears by exciting at 390 nm (see Figs. S33-S35[†]). Finally, unresolved **LEPs** at about 530 nm (Fig. S36[†]) already observed in solution and selectively activated by pumping at 450 nm, are observed as a broad band in time gated measurements (Fig. S37[†]).

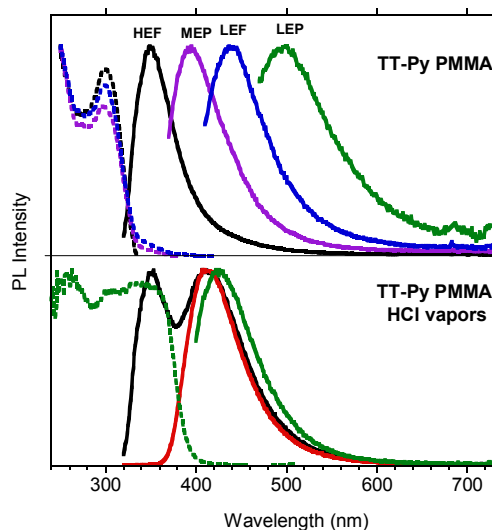


Fig. 4 Top: Photophysical properties of **TT-Py** in PMMA (w/w **TT-Py**/PMMA 10%). $\lambda_{exc}=300$ nm (black line), $\lambda_{exc}=350$ nm (violet line), $\lambda_{exc}=390$ nm (blue line), $\lambda_{exc}=450$ nm (green line) and excitation spectra $\lambda_{em}=352$ nm (black dotted line), $\lambda_{em}=400$ nm (violet dotted line), $\lambda_{em}=440$ nm (blue dotted line). Bottom: Film exposed to HCl vapors ($\lambda_{exc}=300$ nm; black line, 30 min; red line, 45 min; $\lambda_{exc}=390$ nm, green line, 45 min; $\lambda_{em}=527$ nm, green dotted line, 45 min).

To study more in detail these different excited states activated with excitations below 300 nm and at around 390 nm, ultrafast pump-probe measurements have been performed on the blended thin film (w/w **TT-Py**/PMMA 10%). The measured signal is:

$$\frac{\Delta T(\lambda_{PR}, \tau)}{T} = \frac{T_{ON}(\lambda_{PR}, \tau) - T_{OFF}(\lambda_{PR}, \tau)}{T_{OFF}(\lambda_{PR}, \tau)}$$

where T_{ON} and T_{OFF} are the probe transmission intensities with and without pump excitation at a given λ_{PR} and τ probe delay. A positive $\Delta T/T$ signal corresponds to the bleaching of the ground state or stimulated emission (SE) from excited states, while a negative signal indicates the presence of a photoinduced absorption (PIA) band [22].

The $\Delta T/T$ spectra at different probe delays after excitation at the first absorption peak (290 nm) with 20 fs time resolution [23] are reported in the left panel of Fig. 5. The spectra show an initial SE band at around 350 nm and two PIA bands, peaked at 450 nm and 550 nm, PIA₁ and PIA₂ respectively. The temporal evolutions indicate that SE and PIA₂ bands are instantaneously formed, while PIA₁ signal is delayed by about 100 fs with respect to the other two (see Fig. S38[†]). Based on this observation, SE and PIA₂ bands can be assigned to the temporal evolution of the photo-generated excitons which give origin to the **HEF** stimulated emission (S_1-S_0) or to the photoinduced absorption band PIA₂ (S_1-S_n), while the band at



450 nm is associated to the generation of charged states [24]. This result shows the presence of intermolecular interaction between the different molecules. To investigate the origin of the LEF emission, $\Delta T/T$ spectra at different probe delays after excitation at 390 nm (with 100 fs temporal resolution) [25] have been collected (see right panel of Fig. 5). The spectra show an initial PIA band all over the visible spectral region; moreover, at long probe delays, a positive signal appears in the region between 420 nm and 550 nm, indicating emission (supposedly LEF) from a newly formed state. This formation is evident looking at the temporal evolution of the $\Delta T/T$ signal at 450 nm (Fig. S38†) which clearly indicates an initial negative signal which becomes positive in around 700 ps. Moreover, after 1 ns the signal is still growing indicating that the excitation comes from a long living initial excited state and it is likely that this emission will present a long-lived emission tail.

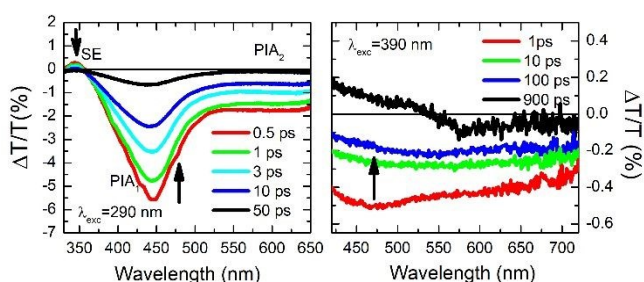


Fig. 5 Ultrafast spectroscopy measurements on TT-Py in PMMA (w/w TT-Py/PMMA 10%). Pump-probe spectra selected at different probe delays after 290 nm (left panel) and 390 nm (right panel) excitations.

We then analyzed the single crystal photoluminescence properties (Table 2). TT-Py crystallizes in three different polymorphs (see Fig. 6). In particular, colorless single crystals are obtained as laminae (TT-Py-A), needles (TT-Py-H) and rectangular blocks (TT-Py-X), by crystallization from $\text{CH}_2\text{Cl}_2/\text{CH}_3\text{OH}$, $\text{CH}_3\text{CN}/\text{H}_2\text{O}$ and CH_3CN respectively. X-ray diffraction analysis reveals that the three polymorphs crystallize in the *Pbcn* (TT-Py-A) and *P2₁/c* (TT-Py-H, TT-Py-X) space groups. TT-Py-H includes in its structure cocrystallized water molecules, that are disordered over three preferential sites. The three polymorphs share the leitmotif of TT moieties' $\pi\cdots\pi$ stacking, already observed in both the TT prototype and its previously investigated derivatives [9, 10, 19-21]. In TT-Py-A, adjacent TT units along the stacks are largely shifted one with respect to the other, as denoted by the distance, 5.358 Å, between respective triazinic centroids. However, several C \cdots C close contacts (3.234, 3.301 Å to cite the shorter ones) are indicative of strong $\pi\cdots\pi$ stacking interactions. Along the stacks, the molecules are slightly rotated one with respect to the other in the plane of TT. In TT-Py-H, adjacent TT units are overlapped without any rotation and display very short slippage (the respective triazinic centroids are separated by 3.736 Å) but slightly longer C \cdots C close contacts (3.309, 3.328 Å). In TT-Py-X, having two molecules in the asymmetric unit, the triazinic centroids of adjacent TT units are alternately separated by 4.756 and 4.917 Å and the shorter C \cdots C contacts measure 3.373 and 3.416 Å. Along the stacks, the molecules

are slightly rotated in the TT's plane, similarly to what observed in TT-Py-A. It should be evidenced that in all the polymorphs, the TT moieties are strongly anchored to each other by not only $\pi\cdots\pi$ stacking interactions but also several short C-H \cdots N hydrogen bonds (HBs) in the plane roughly perpendicular to the stacking axis (the shortest ones measuring 2.44, 2.50 and 2.29 Å in TT-Py-A, -H, and -X, respectively). On the contrary, the pyridine moieties of TT-Py-A and TT-Py-X are involved only in weak C-H \cdots π HBs and N \cdots C close contacts. In TT-Py-H, though the pyridinic nitrogen atom is hydrogen bonded with the disordered cocrystallized water molecules, the high mobility of the latter could not support a rigid environment for the pyridinic ring. As a result, the tilting between TT and pyridine is slightly different in the three structures, being easily influenced by the crystal environment. The dihedral angle ω between the two moieties measures 41.47, 43.7 and 37.6/39.6° in TT-Py-A, -H, and -X, respectively, to be compared with the DFT optimized value as computed *in vacuo*, 36.70°. Moreover, a different relative orientation of pyridine with respect to TT is observed in TT-Py-A with respect to TT-Py-H and TT-Py-X, as indicated by the N7-C10-C2-C1 torsion angle, τ , that measures -35.18° in the former and 41.51 and 34.16/34.64° in the latter structures, respectively.

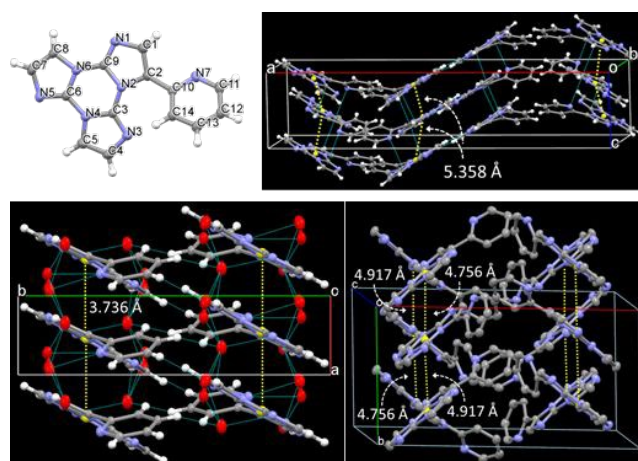


Fig. 6 Top: Asymmetric unit of TT-Py-A and its crystal packing. Bottom: Crystal packing of TT-Py-H (left) and TT-Py-X (right). The centroids of triazinic rings, together with their separation, are shown in yellow. Ellipsoids at 30% probability.

Steady state emission spectra of crystals of TT-Py-A at 298 K in air show an intense high energy ultralong lived emission at 370 nm (HEP, τ_{av} = 0.7 s, Fig. S40†) with an impressive quantum efficiency equal to 52% when excited in the 270-380 nm range (Fig. 7). However, based on the observation of multiple emissions in solution and blended film, we have excited the crystals at longer wavelengths. Broad emissions centered at 450 (LEF) and 524 nm (LEP) are observed when exciting at 390 and 460 nm respectively. From time-gated spectra (Fig. 7 bottom) different phosphorescent contributions can be resolved by analyzing different delay times. At delays longer than 1 ms, the HEP peaked at 370 nm decreases in intensity and the spectral shape evolves revealing a contribution at



about 420 nm (**MEP**; τ_{av} = 0.29 ms) and a longer-lived broad **LEP** at 575–615 nm (τ_{av} = 2.09 ms, Fig. S41[†]).

Similar results are obtained for **TT-Py-H**, (see Fig. 8,) with a **HEP**, **LEF** and **LEP** at 374, 450 and 520 nm (20.38 ms, 1.91 ns and 18.25 ms, respectively, Fig. S43–S45[†]). From time-gated spectra, the **HEP** peaked at 375 nm evolves into **MEP** (τ_{av} = 0.47 ms, Fig. S46[†]) and the structured **LEP-1** at delays longer than 1 ms (λ_{exc} = 320 nm, 535, 570 and 625 nm; τ_{av} = 5.98 ms, Fig. S47[†]). When crystals of **TT-Py-H** are analysed at 77 K (see Fig. 9), **HEF**, **HEP**, **LEF** and **LEP-2** (345, 373, 392, 420 and 493 nm) are resolved. In time gated spectra **MEP** and **HEP** emissions overlap, while, as previously observed in CH_2Cl_2 , the spectral profile of **LEP-1** is selectively activated by exciting at 400 nm.

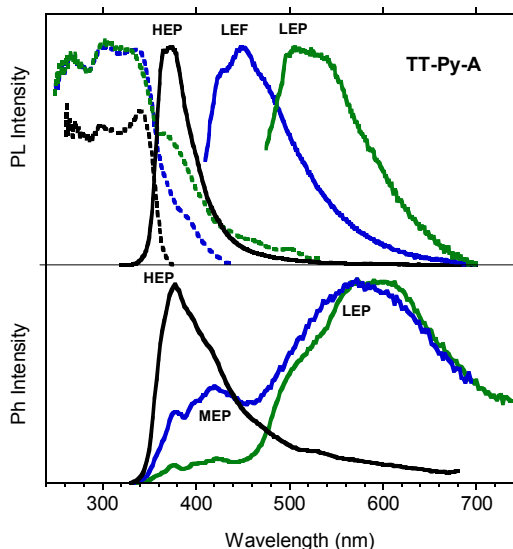


Fig. 7 PL (top) and phosphorescence (bottom) spectra of crystals of **TT-Py-A** at 298 K. Top: Emission spectra (solid lines, λ_{exc} = 300 nm, black line; λ_{exc} = 390 nm, blue line, λ_{exc} = 460 nm, green line) and excitation spectra (dotted lines, λ_{em} = 390 nm, black line; λ_{em} = 460 nm, blue line; λ_{em} = 550 nm, green line). Bottom: Phosphorescence spectra (λ_{exc} = 290 nm; delay 200 μs , window 500 μs , black line; delay 1 ms, window 3 ms, blue line; delay 5 ms, window 10 ms, green line).

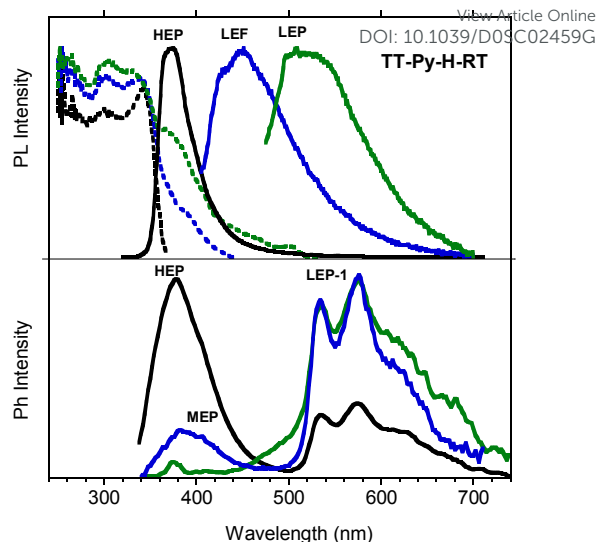


Fig. 8 PL (top) and phosphorescence (bottom) spectra of crystals of **TT-Py-H** at 298 K. Top: Emission spectra: λ_{exc} = 300 nm (black line), λ_{exc} = 390 nm (blue line), λ_{exc} = 460 nm (green line) and excitation spectra λ_{em} = 390 nm (black line), λ_{em} = 460 nm (blue line), λ_{em} = 550 nm (green line). Bottom: Phosphorescence spectra (λ_{exc} = 320 nm; delay 50 μs , window 200 μs , black line; delay 100 μs , window 200 μs , blue line; delay 1 ms, window 10 ms, green line).

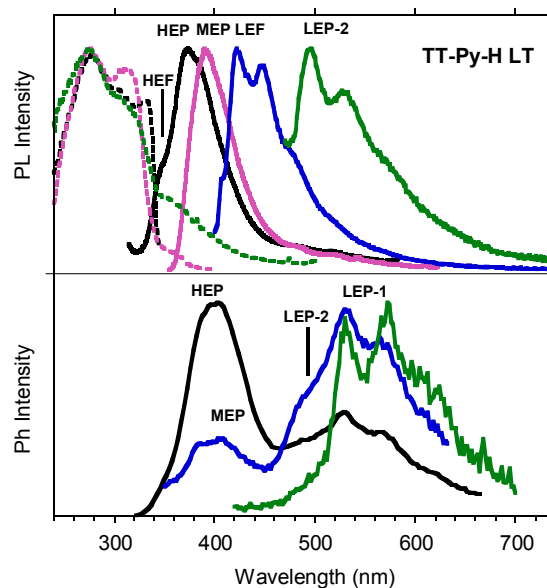


Fig. 9 PL (top) and phosphorescence (bottom) spectra of crystals of **TT-Py-H** at 77 K. Top: Emission spectra λ_{exc} = 300 nm (black line), λ_{exc} = 350 nm (pink line), λ_{exc} = 380 nm (blue line), λ_{exc} = 450 nm (green line) and excitation spectra λ_{em} = 356 nm (black dashed line), λ_{em} = 410 nm (pink dashed line), λ_{em} = 520 nm (green dashed line). Bottom: Phosphorescence spectra at delay 100 μs , window 500 μs (λ_{exc} = 300 nm, black line; λ_{exc} = 330 nm, blue line; λ_{exc} = 400 nm, green line).



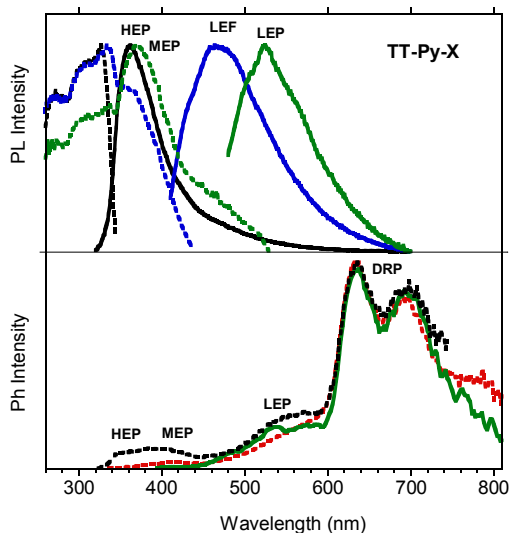


Fig. 10 PL (top) and phosphorescence (bottom) spectra of crystals of **TT-Py-X** at 298 K. Top: Emission spectra $\lambda_{\text{exc}} = 300$ nm (black line), $\lambda_{\text{exc}} = 390$ nm (blue line), $\lambda_{\text{exc}} = 460$ nm (green line) and excitation spectra $\lambda_{\text{em}} = 360$ nm (black dashed line), $\lambda_{\text{em}} = 390$ nm (blue dashed line), $\lambda_{\text{em}} = 460$ nm (green dashed line), $\lambda_{\text{em}} = 550$ nm (green dashed line). Bottom: Phosphorescence spectra ($\lambda_{\text{exc}} = 300$ nm; delay 100 μs , window 500 μs , black dashed line; delay 0.5 ms, window 10 ms, red dashed line; $\lambda_{\text{exc}} = 370$ nm, delay 200 μs , window 500 μs , green line).

Steady state emission spectra of crystals of **TT-Py-X** at 298 K in air display **HEP**, **LEF** and **LEPs** (at 362, 466 and 524 nm, $\tau_{\text{av}} = 91.83$ ms, 4.13 ns and 9.38 ms, respectively, see Fig. 10 top and Fig. S49-S50[†]), similar to the previous phases while their phosphorescence appears more complex. In fact, in time-gated spectra (Fig. 10 bottom) a structured long-lived deep red phosphorescence (**DRP** at 636, 695 and 767 nm, $\tau_{\text{av}} = 111.07$ ms, Fig. S51[†]) dominates the spectrum at delays longer than 0.1 ms. The **HEP** is observed only at short delays (0.1 ms) while longer lived **MEP** at 400 nm and **LEP** at about 530 nm ($\tau_{\text{av}} = 1.31$ ms and 22.60 ms, respectively, Fig. S52-S53[†]) are observed, the latter revealing vibronic replicas similar to those observed for **TT-Py-H** crystals.

The photophysical results on our target, **TT-Py**, highlight the presence of multiple fluorescent and phosphorescent emissions. In particular, two fluorescences (**HEF** and **LEF**) and four phosphorescences (**HEP**, **MEP**, **LEPs** and **DRP**) have been identified according to the experimental conditions and physical state of the sample. Among these, in agreement with our previous findings and based on their photophysical parameters (shape, position and lifetime), **LEPs** and **DRP** seem to be reasonably attributed to dimeric or supramolecular columnar π - π interactions among **TT** units. The **LEP** components, the only visible together with the **HEF** in all phases, appear even in diluted (10^{-5} M) CH_2Cl_2 and CH_3CN solutions where the presence of aggregated species cannot be totally excluded [26]. Accordingly, geometry optimization of dimeric species extracted from the three crystal structures converge on different but almost isoenergetic stationary states characterized by large interaction energies (11.92 kcal/mol BSSE-corrected, for the most stable one). **LEP-1** and **LEP-2** may derive from interacting **TT-Py** units with different

conformations and/or relative orientations [27], as supported by the observation of crystallization of **TT-Py** in three different polymorphs. On the other hand, the **DRP**, which is observed only for **TT-Py-X** crystals, is to be related to a more specific interchromophoric interaction. By analyzing the X-ray structures of the three polymorphs, it is evident that **TT-Py-X** and **TT-Py-H** share the highest H-aggregated character. However, in **TT-Py-H** the co-crystallized water molecules may play the role of vibrational quencher of this low energy emission [28].

The remaining emissions, namely **HEF**, **HEP**, **MEP** and **LEF**, seem to be originated from molecular electronic states (vide infra) even though, some of them, are activated only when rigidification is achieved through intermolecular interactions. In particular, **LEF** is visible only in the solid state (blended films and crystals of all polymorphs).

Particularly relevant in considering the molecular origin of these emissions is the comparison with the analogue **TT-4pyF** compound [21]. For this latter, a photophysical behavior comprising one fluorescence (deactivation from S_1) together with a molecular phosphorescence of T_1 - S_0 origin at about 420 nm and a long lived T_1 - S_0 H-aggregated supramolecular component at about 560 nm, has been observed. In agreement, the **HEF** band of **TT-Py** can be explained by deactivation from S_1 and the compound's **MEP** could be as well interpreted as originated from T_1 as also supported by theoretical calculations (see discussion below). More puzzling is the nature of the remaining emissions, **LEF** and **HEP**, which have been rationalized with the aid of DFT and TDDFT calculations on the optimized molecular geometry of **TT-Py**. Energy scan calculations around the single bond connecting **TT** with pyridine (see Fig. 11) reveal the presence of the two isoenergetic minima corresponding to the observed conformations with the pyridinic N atom 'below' (polymorph **A**) or 'above' the plane of **TT** (polymorphs **H**, **X**). The two minima are separated by a very low barrier (**B**). Another local minimum (**D**), higher by only ~ 1 kcal/mol than the absolute one, corresponds to the conformation with the pyridinic N atom close to the **TT** one. Though this local minimum is not observed in any of the polymorphs of **TT-Py**, its occurrence could not be ruled out in solution, owing to the low (~ 2 kcal/mol) barrier (**C**) from the absolute minimum. Finally, a rotation barrier as high as 7 kcal/mol (**E**) corresponds to the conformation where two nitrogen atoms (one from **Py** and the other from **TT**) face one against the other.



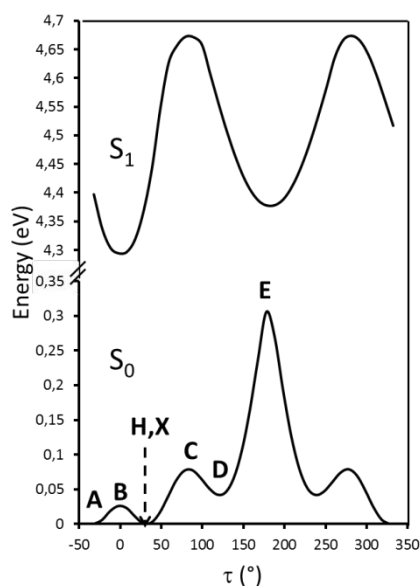


Fig. 11 Scan of the relaxed potential energy surface of the S_1 and S_0 states of **TT-Py** along the N7-C10-C2-C1 torsion angle, τ , at the (TD)- ω B97X/6-311++G(d,p) level of theory. Energies are relative to the S_0 state equilibrium geometry. **A**, **H** and **X** refer to the optimized molecular structures of **TT-Py-A**, **-H**, and **-X**, respectively. **B**, **C**, **D** and **E** denote the other stationary states.

The simulated absorption spectrum of **TT-Py** (see Fig. S56[†] and Table S2), as derived by convolution of the singlet excitation energies computed at the absolute minimum geometry (**A** conformation) well reproduces the UV spectrum. In fact it shows two bands mainly corresponding to the S_0 - $S_{1,A}$ (256 nm, oscillator strength $f = 0.478$) and the S_0 - $S_{7,A}$ (207 nm, $f = 0.428$), both of $^1(\pi, \pi^*)$ character, with intermediate weaker transitions of $^1(\sigma, \pi^*)$, $^1(\sigma/\pi, \pi^*)$ and $^1(\pi, \pi^*)$ character. Here the σ contribution is due to occupied MOs essentially localized on one **TT** nitrogen atom. Though such maxima are blue-shifted with respect to the experimental ones, their separation, equal to 1.16 eV, well matches the observed one, 1.05 eV. Close to $S_{1,A}$, two triplet states are computed with proper symmetries to allow easy ISC from $S_{1,A}$, i.e. $T_{7,A}$ (254 nm, almost overlapped to $S_{1,A}$) with $^3(\sigma/\pi, \pi^*)$ character and $T_{6,A}$ (278 nm) having $^3(\sigma, \pi^*)$ character. Such triplet states could be associated with the **HEP** observed in the emission spectrum.

Further analysis on the levels of **TT-Py** shows that a triplet state ($T_{9,A}$, 254 nm) having $^3(\pi, \pi^*)$ character is computed, close to $S_{2,A}$ (241 nm, oscillator strength $f = 0.021$) of $^1(\sigma, \pi^*)$ character. This explains the slower **MEP** from $T_{1,A}$, having the same $^3(\pi, \pi^*)$ character as $T_{9,A}$, from which it is populated by internal conversion (see modified Jablonski diagram, Fig. 12).

Manifestation of anti-Kasha behavior [29] due to **HEP** emission from $T_{6,A}$ is to be associated with its $(\sigma/\pi, \pi^*)$ symmetry which is different from the (π, π^*) one of $T_{1,A}$. In agreement, for **TT-4pyF** lacking the **HEP**, the computed triplet states close to S_1 have the same symmetry $(\sigma/\pi, \pi^*)$ as T_1 so that internal conversion to this state is always observed producing only a lower energy molecular phosphorescence.

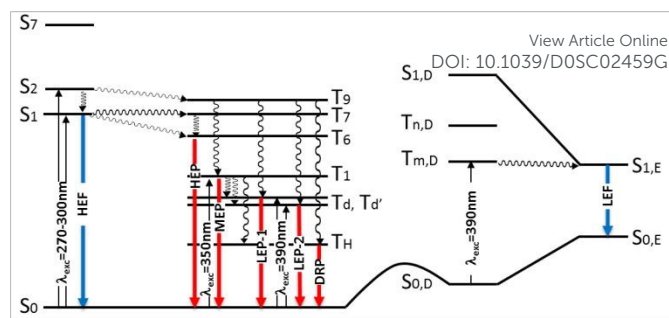


Fig. 12 Schematic photophysical processes of **TT-Py** (fluorescences and phosphorescences shown as blue and red arrows, respectively).

Geometry optimization of the first singlet excited state $S_{1,A}$ of (π, π^*) character leads to a planar conformation corresponding to the '**B**' geometry of the ground state, at only slightly lower energy with respect to the Franck-Condon one. Emission from this state can be associated with the strong **HEF** observed in solution, films and solid state at 350-370 nm when exciting at 270-300 nm. On the other hand, calculations of excitation energies at the local minimum's geometry (point '**D**', see Table S3) provides the $S_{0,D}$ - $S_{1,D}$ transition (of mixed $(\sigma/\pi, \pi^*)$ character) at higher energy with respect to that computed for '**A**', indicating that molecules which happen to be found in this conformation cannot reach their $S_{1,D}$ state using the same values (270-300 nm) of excitation energies. However, geometry optimization of $S_{1,D}$ leads to the planar conformation corresponding to the ground state's '**E**' geometry and associated with much lower energy than the Franck-Condon one (see Table S4). Emission from this optimized $S_{1,E}$ state could explain the **LEF** observed in films and solid state at 450 nm when exciting at 390 nm. Such lower excitation energy, in fact, allows for population of a triplet state with the proper (π, π^*) symmetry which crosses $S_{1,E}$ and finally decays on the ground state. A $S_{0,D} \rightarrow T_{m,D} \rightarrow S_{1,E} \rightarrow S_{0,E}$ mechanism has to be invoked since no singlet states are computed at such low (390 nm) energy neither for the molecule (see Tables S2-S4) nor for its dimeric aggregates (see Tables S5-S7).

These conclusions are in agreement with the pump-probe results shown in the right panel of Fig. 5. Upon pumping directly the $T_{m,D}$ triplet state (recognizable in the spectrum from the negative PIA band $T_{m,D} \rightarrow T_{n,D}$) the $S_{1,E}$ state responsible for the **LEF** emission is populated by intersystem crossing [24]. Such process is in principle present also when exciting at higher energy (for example by activating **D** conformer from $S_{0,D}$ to $S_{1,D}$) but could not be observed because obscured by the much more efficient **HEF** emission. Moreover, its observation only in films and crystals suggests that it can be switched on only in rigidified environment. Finally, it requires that even in the crystalline state a portion of molecules should be found in the **D** conformation, this condition could be realized both as defects in the crystalline structure and on the crystal surfaces.

To acquire further information to be used in completing the puzzle of such intricate photophysical behavior, we exposed the **TT-Py** PMMA film to acidic vapors. In fact, it is expected that the protonation of the nitrogen atom on the pyridine



moiety should block the free rotation around the bond connecting **TT** and pyridine. 30 min exposure to HCl vapors are not enough to get full protonation of the pyridinic fragment, as revealed by the steady state emission spectrum of the film (see Fig. 4 bottom) which displays both the high energy fluorescence of **TT-Py** together with the additional intense red shifted fluorescence (412 nm, τ_{av} = 3.56 ns, Fig. S54[†]) of **TT-PyH⁺**. After 45 min, however, the original fluorescence has completely disappeared and only the 412 nm component is visible. By exciting at 390 nm a phosphorescence at 425 nm (τ_{av} = 13.94 ms, Fig. S55[†]) is observed in the spectrum of the film while the 450 nm **LEF** of **TT-Py** is missing. The original spectrum is restored by exposing the film of **TT-PyH⁺** to NH₃ vapors.

Geometry optimization of **TT-PyH⁺**, starting from the minimum energy conformation of **TT-Py** where a proton has been added on the more basic pyridine nitrogen, leads to a stationary point which actually reveals to be a metastable conformation (Fig. 13). A relaxed energy scan of **TT-PyH⁺**, in fact, shows that a much more stable (>10 kcal/mol) minimum is observed when the pyridinic protonated nitrogen atom and the one on **TT** are facing each other, according to a geometry reminiscent of the proton sponges' one [30]. The two minima are separated by a low (~2 kcal/mol) energy barrier, indicating a quantitative transformation from the higher to the lower energy minimum at room temperature. TDDFT calculations have been then performed on the more stable conformation of **TT-PyH⁺**, confirming the red-shifted fluorescence observed experimentally (see Table S8 and Fig. S56[†]). Importantly, the absence of the low energy fluorescence at 450 nm is predicted by the rigidity of the **TT-PyH⁺** scaffold.

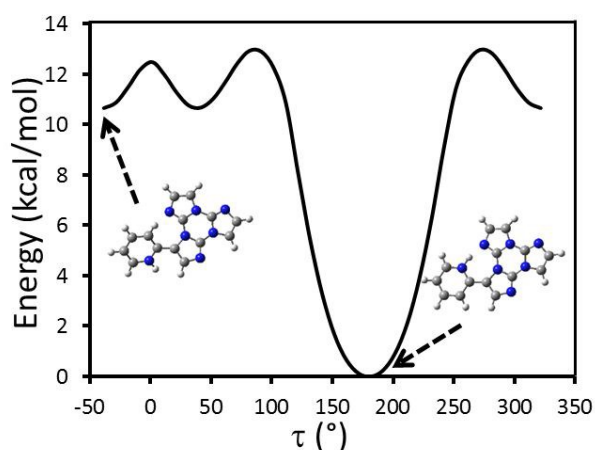


Fig. 13 Scan of the relaxed potential energy surface of **TT-PyH⁺** along the N7-C10-C2-C1 torsion angle, τ , at the (TD)- ω B97X/6-311++G(d,p) level of theory. Energies are relative to the minimum energy geometry.

Conclusions

A new single-component AIE material, based on the simple 3-(pyridin-2-yl)triazotriazine (**TT-Py**) organic molecule, is

here reported. Under ambient conditions, it shows excitation-dependent fluorescence and phosphorescence in both blended film and three different crystalline phases. In particular, **HEF**, **HEP**, **MEP** and **LEF** emissions of molecular origin, together with **LEPs** and **DRP** aggregated RTPs, can be activated by proper excitation wavelength thus covering the entire visible region.

This color-tunable property derives, in a combined way, from the specific aggregation features of the **TT** scaffold on one side and, on the other, from the relative conformational freedom of the pyridinic pendant and the peculiar position of its nitrogen atom (in ortho with respect to **TT**). More precisely, strong π - π stacking interactions among **TT** moieties and very short C-H...N hydrogen bonds, granting high molecular rigidity, provide the prerequisites for long-lived luminescence of aggregated (red and deep red RTPs) and molecular (blue and green RTPs, according to the symmetry of the excited state) origin, respectively. Moreover, the partial mobility of the pyridinic fragment is responsible not only for the low-energy fluorescence, originated from a distinctive shape of ground and excited state potential energy surfaces, but also for multiple aggregated-derived RTPs, associated with the presence of different aggregation motifs of stable and metastable states.

Such an extremely rich photophysical behavior of **TT-Py**, together with its implementation in flexible films allowing easy fabrication and processability, make the proposed material a promising platform for applications in information storage, security encryption, sensing and display.



Table 1 Photophysical parameters of **TT-Py** in solution.

Sample	298 K					77 K			*time gated spectra
	Φ (%)	λ_{abs} (nm)	λ_{em} (nm)	τ_{av}	Origin	λ_{em} (nm)	τ_{av}	Origin	
CH₂Cl₂	17	237, 290	351	0.62 ns	HEF S ₁ -S ₀	325, 345	2.32 ns	HEF S ₁ -S ₀	
				10.2 ms	HEP T ₆ -S ₀	375	13.16 ms	HEP T ₆ -S ₀	
			408 420*	11.01 ms 40 μ s*	MEP T ₁ -S ₀	393		MEP T ₁ -S ₀	
			500 520, 562, 615*	12.04 ms 441 μ s*	LEP-1 T _d -S ₀	485, 518, 550*	1.31 s	LEP-2 T _d -S ₀	
CH₃CN	15	233, 285	355	1.36 ns	HEF S ₁ -S ₀	343	2.46 ns	HEF S ₁ -S ₀	
				43.47 ms	HEP T ₆ -S ₀	388	17.79 ms	HEP T ₆ -S ₀	
			488, 521, 560	0.28 ms*	LEP-2 T _d -S ₀	500	889 ms	LEP-2 T _d -S ₀	
CH₃CN/H₂O		233, 280	345	79.13 ms	HEP T ₆ -S ₀				
			380-420		MEP T ₁ -S ₀				
			486, 515, 556 515, 556, 610*	24.00 ms	LEP-1 T _d -S ₀ LEP-2 T _d -S ₀				



Table 2 Photophysical parameters of **TT-Py** in the solid state.

Sample	298 K				
	Φ (%)	λ_{obs} (nm)	λ_{em} (nm)	τ_{av}	Origin
PMMA film		223, 293	350	1.18 ns	HEF S_1-S_0
			394	13.73 ms	MEP T_1-S_0
			440	3.47 ns	LEF $S_{1,E}-S_{0,E}$
			530	15.70 ms	LEP T_d-S_0
TT-Py-A	52		370	698 ms	HEP T_6-S_0
			418*	0.29 ms*	MEP T_1-S_{00}
			450		LEF $S_{1,E}-S_{0,E}$
			510,570,608*	2.09 ms*	LEP T_d-S_0
TT-Py-H			374	20.38 ms	HEP T_6-S_0
			408*	0.47 ms*	MEP T_1-S_{00}
			450	1.91 ns	LEF $S_{1,E}-S_{0,E}$
			500 528,562,610*	18.25 ms 5.98 ms*	LEP T_d-S_0
TT-Py-X			362	91.83 ms	HEP T_6-S_0
			402*	1.31 ms*	MEP T_1-S_0
			466	4.13 ns	LEF $S_{1,E}-S_{0,E}$
			524 536,585*	9.38 ms 22.60 ms*	LEP T_d-S_0
			636, 695,767*	111.1 ms*	DRP T_H-S_0

*time gated spectra



Conflicts of interest

There are no conflicts to declare.

Acknowledgements

The use of instrumentation purchased through the Regione Lombardia-Fondazione Cariplo joint SmartMatLab Project is gratefully acknowledged. A.F. thanks Mr. Pietro Colombo for support in single crystal X-ray data collection. TV and LG acknowledge the financial support from the Regione Lombardia project "I-Zeb".

Notes and references

- W. Qin, P. Zhang, H. Li, J. W. Y. Lam, Y. Cai, R. T. K. Kwok, J. Qian, W. Zheng and B. Z. Tang, *Chem. Sci.*, 2018, **9**, 2705.
- L. Gu, H. Wu, H. Ma, W. Ye, W. Jia, H. Wang, H. Chen, N. Zhang, D. Wang, C. Qian, Z. An, W. Huang and Y. Zhao, *Nat. Commun.*, 2020, **11**, 944.
- R. Gao and D. Yan, *Chem. Commun.*, 2017, **53**, 5408.
- S. Hirata, K. Totani, H. Kaji, M. Vacha, T. Watanabe and C. Adachi, *Adv. Opt. Mater.*, 2013, **1**, 438.
- W. Zhao, Z. He, J. W. Y. Lam, Q. Peng, H. Ma, Z. Shuai, G. Bai, J. Hao and B. Z. Tang, *Chem*, 2016, **1**, 592.
- S. Xu, Y. Duan and B. Liu, *Adv. Mater.*, 2020, **32**, 1903530.
- P. Alam, N. L. C. Leung, J. Liu, T. S. Cheung, X. Zhang, Z. He, R. T. K. Kwok, J. W. Y. Lam, H. H. Y. Sung, I. D. Williams, C. C. S. Chan, K. S. Wong, Q. Peng and B. Z. Tang, *Adv. Mater.*, 2020, 2001026.
- Z. An, C. Zheng, Y. Tao, R. Chen, H. Shi, T. Chen, Z. Wang, H. Lin, R. Deng, X. Liu and W. Huang, *Nat. Mater.*, 2015, **14**, 685.
- E. Lucenti, A. Forni, C. Botta, L. Carlucci, C. Giannini, D. Marinotto, A. Previtali, S. Righetto and E. Cariati, *J. Phys. Chem. Lett.*, 2017, **8**, 1894.
- E. Lucenti, A. Forni, C. Botta, L. Carlucci, C. Giannini, D. Marinotto, A. Pavanello, S. Righetto and E. Cariati, *Angew. Chem. Int. Ed.*, 2017, **56**, 16302.
- R. Kabe and C. Adachi, *Nature*, 2017, **550**, 384.
- O. Bolton, K. Lee, H.-J. Kim, K. Y. Lin and J. Kim, *Nat. Chem.*, 2011, **3**, 205.
- H. Shi, Z. An, P.-Z. Li, J. Yin, G. Xing, T. He, H. Chen, J. Wang, H. Sun, W. Huang and Y. Zhao, *Cryst. Growth Des.*, 2016, **16**, 808.
- Z. Lin, R. Kabe, N. Nishimura, K. Jinnai and C. Adachi, *Adv. Mater.*, 2018, **8**, 1803713.
- L. Gu, H. Shi, L. Bian, M. Gu, K. Ling, X. Wang, H. Ma, S. Cai, W. Ning, L. Fu, H. Wang, S. Wang, Y. Gao, W. Yao, F. Huo, Y. Tao, Z. An, X. Liu and W. Huang, *Nat. Photonics*, 2019, **13**, 406.
- Z. Wang, Y. Zhang, C. Wang, X. Zheng, Y. Zheng, L. Gao, C. Yang, Y. Li, L. Qu and Y. Zhao, *Adv. Mater.*, 2020, **32**, 1907355.
- C. J. Chen, Z. G. Chi, K. C. Chong, A. S. Batsanov, Z. Yang, Z. Mao, Z. Y. Yang and B. Liu, *ChemRxiv. Preprint*, DOI: doi.org/10.26434/chemrxiv.9895724.v1.
- A. P. Demchenko, V. I. Tomin and P.-T. Chou, *Chem. Rev.*, 2017, **117**, 13353.
- E. Lucenti, A. Forni, C. Botta, L. Carlucci, A. Colombo, C. Giannini, D. Marinotto, A. Previtali, S. Righetto and E. Cariati, *ChemPhotoChem*, 2018, **2**, 801.
- E. Lucenti, A. Forni, C. Botta, C. Giannini, D. Malpicci, D. Marinotto, A. Previtali, S. Righetto and E. Cariati, *Chem. Eur. J.*, 2019, **25**, 2452.
- A. Previtali, E. Lucenti, A. Forni, L. Mauri, C. Botta, C. Giannini, D. Malpicci, D. Marinotto, S. Righetto and E. Cariati, *Molecules*, 2019, **24**, 2552.
- G. Cerullo, C. Manzoni, L. Lüer and D. Polli, *Photochem. Photobiol. Sci.*, 2007, **6**, 135.
- R. Borrego-Varillas, L. Ganzer, G. Cerullo and C. Manzoni, *Appl. Sci.*, 2018, **8**, 989.
- O. Svelto, *Principles of Lasers*, Springer, Boston, MA, 5th edn., 2010.
- A. Portone, L. Ganzer, F. Branchi, R. Ramos, M. J. Caldas, D. Pisignano, E. Molinari, G. Cerullo, L. Persano, D. Prezzi and T. Virgili, *Sci. Rep.*, 2019, **9**, 7370.
- H. Kang, A. Facchetti, P. Zhu, H. Jiang, Y. Yang, E. Cariati, S. Righetto, R. Ugo, C. Zuccaccia, A. Macchioni, C. L. Stern, Z. Liu, S.-T. Ho and T. J. Marks, *Angew. Chem. Int. Ed.*, 2005, **44**, 7922.
- Y. Wang, J. Yang, Y. Tian, M. Fang, Q. Liao, L. Wang, W. Hu, B. Z. Tang and Z. Li, *Chem. Sci.*, 2020, **11**, 833.
- J.-C. G. Bünzli and C. Piguet, *Chem. Soc. Rev.*, 2005, **34**, 1048.
- Y.-H. Wu, H. Xiao, B. Chen, R. G. Weiss, Y.-Z. Chen, C.-H. Tung and L.-Z. Wu, *Angew. Chem. Int. Ed.*, doi:10.1002/anie.202000608.
- A. L. Llamas-Saiz, C. Foces-Foces and J. Elguero, *J. Mol. Struct.*, 1994, **328**, 297.



View Article Online
DOI: 10.1039/D0SC02459G

Open Access Article. Published on 09 June 2020. Downloaded on 6/9/2020 8:17:49 AM.
This article is licensed under a Creative Commons Attribution-NonCommercial 3.0 Unported Licence.



Chemical Science Accepted Manuscript

TT-Py exhibits anti-Kasha and multiple emissive behaviour due to the copresence of rigid **TT** and partially conformationally free **Py**

View Article Online
DOI: 10.1039/D0SC02459G

